

Scandium modified zirconia extracted from red mud as a waste of alumina production

Liliya A. Pasechnik, Irina S. Medyankina, Danil I. Pereverzev, Alexander Yu. Chufarov, Alexey Yu. Suntsov

Institute of Solid State Chemistry UB RAS, Ekaterinburg, Russia

Corresponding author: L.A. Pasechnik, pasechnik@ihim.uran.ru

ABSTRACT The total or partial utilization or recycling of bauxite processing waste (red mud) has the potential to reduce the harmful effect on the environment while simultaneously extracting the most valuable ingredient, scandium which is currently underutilized due to its high cost. The new efficient carbonation technology promises an assured supply of scandium and zirconium at a significantly reduced cost. Here, scandium-zirconium concentrate, extracted by hydrolysis from leachate after carbonate treatment of red mud, was subjected to sintering by ceramic technology at 1100 °C to produce scandia-stabilised zirconia (ScSZ). The XRD patterns demonstrate the successful doping of scandium into the zirconia lattice through the hydrolytic precipitation method. The ratio between the essential components of the functional ceramics Zr and Sc is approximately 4, which correlates with the doping level of ScSZ up to $Zr_{0.8}Sc_{0.2}O_{1.9}$.

KEYWORDS zirconia oxide, Sc–Zr concentrate, ScSZ, zirconium ceramics, thermal expansion, red mud

ACKNOWLEDGEMENTS The work was supported by RCF and Government of the Sverdlovsk region, project No. 24-29-20278, <https://rscf.ru/en/project/24-29-20278/>

FOR CITATION Pasechnik L.A., Medyankina I.S., Pereverzev D.I., Chufarov A.Yu., Suntsov A.Yu. Scandium modified zirconia extracted from red mud as a waste of alumina production. *Nanosystems: Phys. Chem. Math.*, 2024, **15** (6), 768–773.

1. Introduction

Zirconium oxide and ceramic materials based on it are widely employed in engineering and medicine due to their high refractory properties, strength, chemical inertness, superionic oxygen conductivity, as well as their biocompatibility and catalytic activity [1–5]. Yttrium-stabilized zirconia (YSZ) is commonly used material in solid oxide fuel cells (SOFC) for high temperature applications [6]. Scandia stabilized zirconia (ScSZ) exhibits conductivity that is 1.5 – 3 times superior to that of YSZ, due to its distinctive crystal structure [7]. At the same time Sc-containing materials are not commonly used as functional ceramic due to high cost but small additives appear to be effective for the increased ionic conductivity, structural and thermodynamic stability.

It is known that not only the type and amount of additives the size of the initial powders have a significant impact on the process of their sintering, and, as a consequence, on the structure and mechanical properties of ceramics [8,9]. Studies have shown that with the decrease in particle sizes, the physicochemical properties like strength, thermal conductivity, high-temperature resistance, toughness and specific surface area improve, comparing micron-ZrO₂ to nano-ZrO₂ [10, 11]. On the other hand, the physical and mechanical properties change significantly depending on the sintering temperature and the holding time at maximum temperature [12].

At present most widespread methods for preparing initial zirconia particles with a narrow particle size distribution are emulsion method [13], sol-gel combustion [14], spray-drying and spray-pyrolysis [15], solvothermal synthesis [16] and other [17]. In many instances, the raw materials are either costly and toxic organometallic compounds or solutions of inorganic salts utilized for the execution of solvothermal processes with simultaneous or subsequent heat treatment at selected temperatures. A controlled double-jet precipitation is believed to be a rather simple method enabling to govern size, shape and porosity of hydrous zirconia particles maintaining a narrow size distribution of zirconia particles after drying and calcination [18]. A similar relatively simple deposition process of a carbonate-hydrocarbonate solution can be implemented to produce scandium-containing zirconia from red mud – residue from bauxite processing [19]. However, industrial raw materials contain impurities of other metals along with the specified elements [20, 21]. Their presence can be both beneficial to the sintering process and detrimental to the properties of the final material. In this work, the direct cheap creation of ceramics based on scandium-stabilized zirconia (ScSZ) and the assessment of its thermochemical properties are of interest.

2. Experimental

2.1. Extraction of zirconia concentrate

Sc-doped zirconia oxide was produced by hydrolysis of carbonate-hydrocarbonate solution after the carbonation leaching of red mud derived from an alumina plant located in the Ural region (Russia). The detailed description of carbonation processing of red mud with 10 % NaHCO₃ solution or using sintering furnaces (7 – 20 % CO₂) and precipitation of Sc–Zr concentrate are provided earlier [19, 22]. Supplying of carbon dioxide promotes the synthesis of soluble carbonate complexes [Sc(CO₃)₄]⁵⁻ and [(ZrTi)(CO₃)₄]⁴⁻ and starts neutralization processes of alkali from red mud and alkali resulted from the hydrolysis of aluminates, titanates, etc. The carbonate-bicarbonate filtrate at pH = 8 – 9, separated from the insoluble mass of carbonized red mud, contains up to 30 – 50 g/m³ Sc and 250 – 350 g/m³ Zr. Concentrate from the clarified solution was precipitated by sodium hydroxide at heating and holding for 4 or 24 hours to coagulate the precipitate. In this work, the hydrolysis of a carbonate-bicarbonate solution was carried out at 90 – 100 °C to pH 12.5 for 24 h. Before control of the chemical composition both initial red mud and Sc–Zr concentrate were further dried at 125 °C for 24 h (initial moisture content was about 20 – 30 wt %) and comminuted. The respective compositions of initial red mud and the concentrate obtained from hydrochemical branch of the plant are listed in Table 1.

TABLE 1. The compositions of initial red mud and Sc–Zr concentrate

Component	Red mud, % wt.	Sc–Zr concentrate, % wt.
Fe ₂ O ₃	41.0	7.52
Al ₂ O ₃	15.4	0.94
CaO	9.0	4.09
MgO	0.4	2.17
TiO ₂	5.5	8.37
SiO ₂	7.5	1.05
Na ₂ O	5.6	5.89
K ₂ O	0.4	0.41
ZrO₂	0.04	58.87
Sc₂O₃	0.012	10.46

2.2. Methods of characterization

The element content in Sc–Zr concentrate after drying at 125 °C was determined by inductively coupled plasma atomic emission spectroscopy (ICP-AES) using a spectrometer Elan9000 (PerkinElmer).

In order to obtain polycrystalline powders dried concentrates were thoroughly grinded and mixed up in jasper mortar then pressed into disk shape bar and annealed at 600, 800, 1000 and 1100 °C in air during 10 – 12 hours. XRD patterns were collected at room temperature on a Shimadzu XRD-7000 diffractometer using CuK α radiation in the 2 θ range 10° to 70° with a step of 0.03° and exposition 3 s. Polycrystalline silicon ($a = 5.43075(5)$ Å) was used as an external standard. The PDF2 database (ICDD, USA, Release 2016) was applied for phase analysis and the identification of *c*-ZrO₂ (card No. 00-054-1136). Polythermal dependencies were recorded at temperature scan rate of 10 °C/min up to 800 °C, with alumina as a standard.

Microstructure was analyzed by means of scanning electron microscopy method with the use of scanning electron microscope (SEM) VEGA 3 LMH (TESCAN) equipped with energy dispersive analyzer INCA Energy 350/X-max 80 (Oxford Instruments) used for the study of atomic distribution and a scanning electron microscope JEOL-JSM LA 6390 equipped with a JEOL JED-2300 detector.

Thermal expansion was studied on rectangular bar with a section of 5 × 5 mm cut from the sintered sample. Data on linear elongation was collected using L75 (Linseis) dilatometer at heating mode with the rate 3 °/min in air.

3. Results and discussion

The typical SEM-image of the Sc–Zr concentrate produced directly from red mud shown in Fig. 1a reveals that sample consists of homogeneously dispersed very fine near spherical shaped particles with easily crushed micrometer-sized agglomerates. The results of EDX analysis (Fig. 1b) correlate with the concentrations of elements obtained from ICP-AES analysis as shown in Table 1.

The pattern of initial Sc–Zr concentrate with a wide hump between 20° and 40° 2 θ indicates an amorphous nature or nanocrystalline structure of the sample. Calcination at 200 °C to constant mass shows adsorbed and structured moisture of about 25 – 30 wt. %, which is typical of amorphous hydroxide phases with a highly developed surface. The thermal

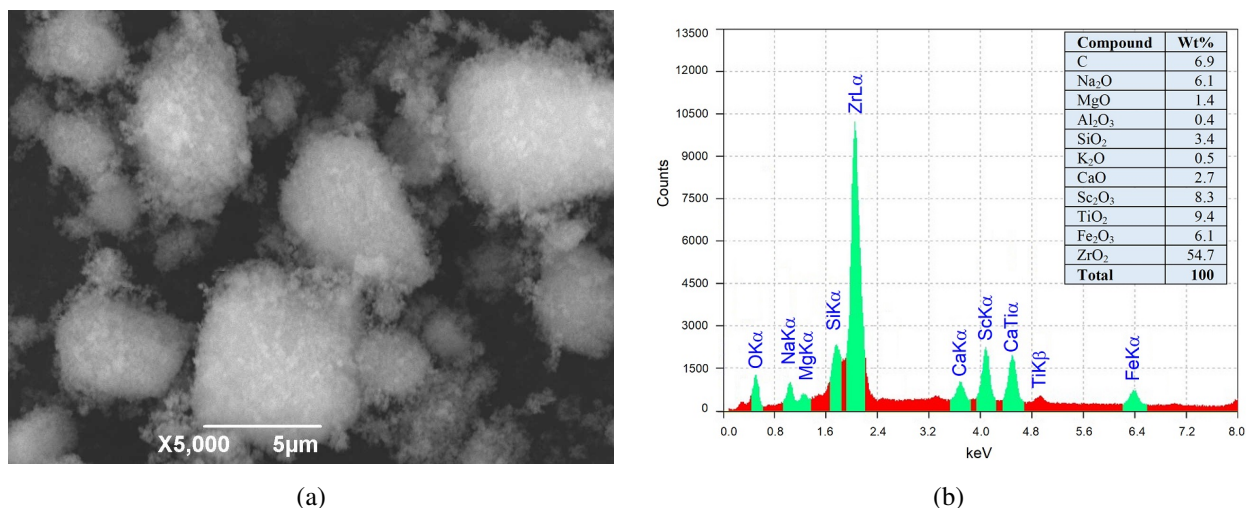


FIG. 1. SEM images (a) and EDX-analysis (b) of initial Sc–Zr concentrate

behavior of Sc–Zr concentrate after heating at 200 °C is shown in Fig. 2a. The total mass loss is pretty much finished after annealing at 600 °C. The rest 1 – 2 % of the mass are lost during the further 9 h of annealing from 600 to 800 °C with the exposition at 800 °C. The calcination of the initial Sc–Zr concentrate for 4 h at 600 °C corresponds to complete decomposition of amorphous hydroxide and carbonate compounds (ScCO₃OH, TiO(OH)₂, ZrO(OH)₂, Sc(OH)₃, Ti(OH)₄, Zr(OH)₄, etc.). From the XRD patterns of calcined samples (Fig. 2b) it is clear that a nanosized composite of the solid solution based on *c*-ZrO₂ (cubic) structure (ICDD Card No. 00-054-1136, pr. gr. Fm $\bar{3}$ m) was obtained [23], with no apparent diffraction peaks corresponding to the *m*-ZrO₂ (monoclinic) phase. The lattice parameters of the fluorite structure *c*-ZrO₂ powders in Table 2 were estimated by the Rietveld refinements. The observed narrowing of the X-ray lines indicates an increase in the size of zirconia particles doped with scandium ions when samples annealed from 600 to 1100 °C. The average value of the crystallite size (*d*) was calculated from X-ray line broadening using Scherrer.

TABLE 2. Variation of the lattice parameters and crystallite size of *c*-ZrO₂ with the calcination temperature

<i>T</i> , °C	Lattice parameter		<i>d</i> , nm
	<i>a</i> , Å	<i>V</i> , cm ³	
600	5.04(1)	128.0(5)	9
800	5.058(6)	129.4(2)	74
1000	5.053(3)	129.0(1)	98
1100	5.074(1)	130.63(3)	>100

Except for orthorhombic perovskite CaTiO₃, no Sc₂O₃ or other impurities were found by X-ray diffraction. These results show that scandium was successfully incorporates into the zirconia lattice by the hydrolysis so-precipitation method. At the same time other components such as iron, alumina and magnesium may also act as dopant in ScSZ for crystal structure stabilization and created functional properties [24–26]. For example, in a compositions with oxides of aluminum, chromium and iron, which are not, in the conventional sense, stabilizers of the *c*-ZrO₂ phase, the formation of 100 % of the cubic phase was establish [27].

For the evaluation of functional properties, the obtained Sc–Zr product was uniaxially pressed and sintered at 1100 °C. Fig. 3a presents the fractured surface morphology of sintered ScSZ ceramic, which shows that some micro pores were uniformly distributed in the area of SEM-image. As seen from Fig. 3b in BEC regime, the grain size is 1 – 3 μm for bulk Sc–Zr product.

Figure 3c demonstrates overall EDS-mapping and partial chemical components of the ceramic samples obtained by splitting. By analyzing Fig. 3c one can see that the most cations are distributed fairly evenly over the surface. It is important that this also applies to key components forming ScSZ. It is worth noting that there are some elements form separate areas, for example, iron and calcium. However, given the low concentration of most components, their presence in the selected pictures allows us to suggest that the cations are statistically distributed throughout the sample bulk.

Table 3 demonstrates compositions determined from EDX analysis (in % at.). As can be seen main component is zirconium. It is important to pay attention to the ratio of Zr and Sc as key components of the functional ceramics. This parameter lies about the value 4 that corresponds to doping state of ScSZ up to Zr_{0.8}Sc_{0.2}O_{1.9}. The obtained result is in

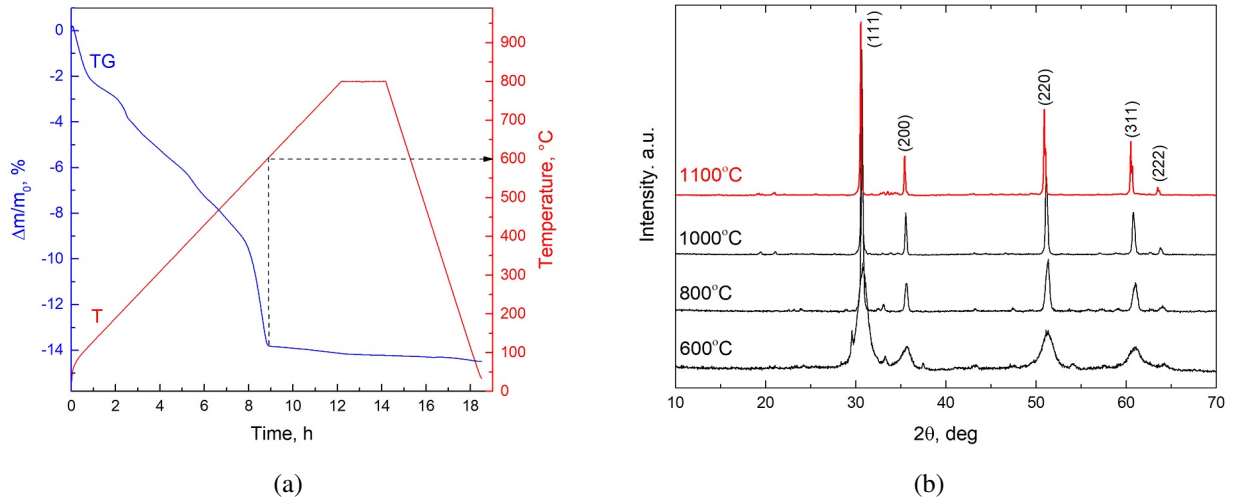


FIG. 2. TG curve (a) and temperature dependent changes of XRD patterns (b) of Sc-Zr powders

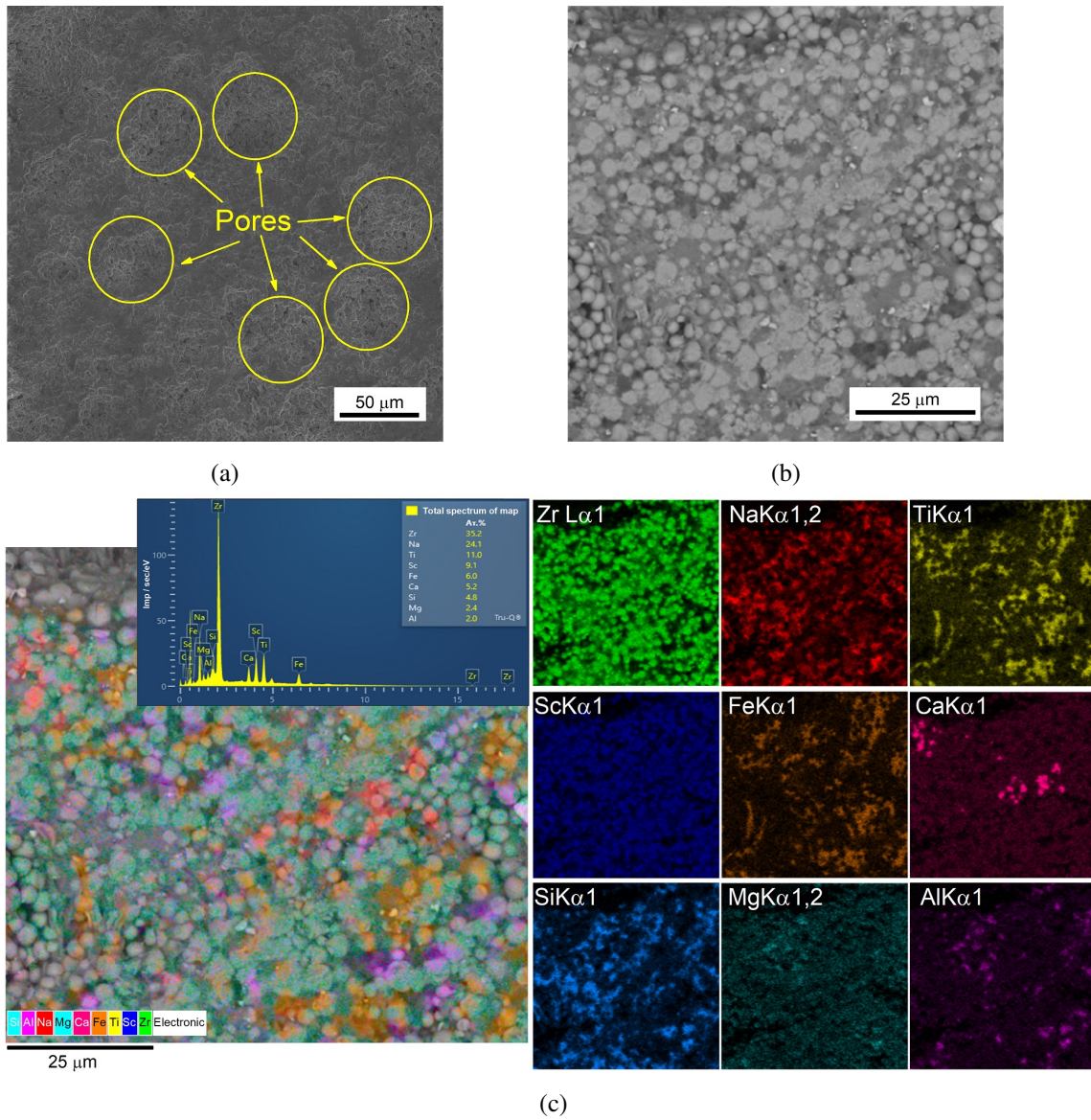


FIG. 3. Surface SEM image of the sintered bulk ScSZ material in regimes SEI (a) and BEC (b) and (c) EDX mapping with corresponding partial cationic distributions over the chipped ceramic obtained from the Sc-Zr concentrate

good agreement with XRD data and is strongly supported by work [23] where a formation of cubic fluorite ScSZ in these doping limits was distinguished as preferable. Accordingly, the applied conditions were found to permit the production of well-sintered ceramics, thereby facilitating subsequent analysis of functional properties. It is assumed that sum quantity of oxide components can act as sintering aids for zirconia ceramics (Al_2O_3 , CaO , MgO , etc) [28, 29], which are used, either individually or in combination, to optimize the properties of ceramic thermal barrier coatings [30, 31].

The change for linear elongations of the studied Sc–Zr ceramics with temperature is represented in Table 4. Additionally, the values of the thermal expansion coefficients for every point k were calculated in accordance with the following formulae:

$$a_{\text{phys}}(k) = \frac{1}{L_0} \frac{d(\Delta L_k)}{dT} \quad \text{and} \quad a_{\text{tech}}(k) = \frac{1}{L_0} \frac{\Delta L_k - \Delta L_0}{T_k - T_0} \quad \text{for } (k = 1 \dots n),$$

where L_0 is the sample length at 20 °C, ΔL_k is the length change at T_k , ΔL_0 is the change in length at 20 °C (linear extrapolated out of the first data point).

TABLE 3. Chemical composition of sintered Sc–Zr ceramics obtained from EDX analysis (at %)

Element	Zr	Sc	Zr/Sc	Na	Ti	Fe	Ca	Si	Mg	Al
Content	35.2	9.1	3.89	24.1	11.0	6.0	5.2	4.8	2.4	2.0

TABLE 4. Thermal expansion coefficient values of the Sc–Zr ceramic materials

$T, ^\circ\text{C}$	Ceramic on $\text{Zr}_{0.8}\text{Sc}_{0.2}\text{O}_{1.9}$		14Sc_1YSZ (mol %)	8Sc_1YSZ (wt %)
	$\alpha_{\text{tech}} \cdot 10^6, \text{K}^{-1}$	$\alpha_{\text{phys}} \cdot 10^6, \text{K}^{-1}$	bulk material [32]	coating [33]
500	10.78	11.91	9.7	10.65
600	10.86	11.98	9.8	10.75
700	11.37	13.11	10.05	10.80
800	11.76	14.53	10.17	10.85
900	11.93	10.55	10.30	10.80

The values of α selected at 500 – 900 °C for comparison with available literature data are provided. It should be noticed that the value of expansion coefficient is in the best coincidences with Sc doped YSZ ceramics both in the coating and in the bulk material. Thus, the present impurity components co-precipitated from the carbonate-bicarbonate solution and the phases formed during sintering did not significantly affect the thermal behavior of Sc–Zr ceramics in the studied temperature range.

4. Conclusion

Sc–Zr ceramics were obtained by ceramic technology from Sc–Zr concentrate produced by co-precipitation method after carbonation of red mud pulp. Scandium oxide was not detected as a single phase, but successfully stabilized the $c\text{-ZrO}_2$ structure (pr. gr. $\text{Fm}\bar{3}\text{m}$) by substitution during sintering of Sc–Zr concentrate. Despite the fact that the main mass loss practically was finished at temperatures above 600 °C the crystallization of scandium-stabilized zirconia continues up to 1100 °C. Analysis of Sc–Zr ceramic has shown that the scandium distribution along the surface is homogeneous and the Sc_2O_3 amount regarding zirconia is almost identical to its content in the concentrate. In conclusion, we have shown that the thermal expansion coefficient values of the ceramic on $\text{Zr}_{0.8}\text{Sc}_{0.2}\text{O}_{1.9}$ phase in the temperature range of 500 – 900 °C are much like to the values for materials from co-doped Sc and Y zirconia. The impurities did not significantly affect the phase composition and thermal behavior of Sc–Zr ceramics obtained by a simple and inexpensive way from the metallurgical waste.

References

- [1] Liu Q., Huang, S., He, A. Composite ceramics thermal barrier coatings of yttria stabilized zirconia for aero-engines. *J. Mater. Sci. Technol*, 2019, **35**, P. 2814–2823.
- [2] Vinchhi P., et al. Recent advances on electrolyte materials for SOFC: A review. *Inorg. Chem. Commun.*, 2023, **152**, 110724.
- [3] Soon G., et al. Review of zirconia-based bioceramic: Surface modification and cellular response. *Ceram. Int.*, 2016, **42**, P. 12543–12555.
- [4] Basahel S.N., et al. Influence of crystal structure of nanosized ZrO_2 on photocatalytic degradation of methyl orange. *Nanoscale Res. Lett.*, 2015, **10**, 73.
- [5] Pushpalatha S., et al. Green synthesis of cellulose/ ZrO_2 nanocomposite: assessment of antibacterial and photocatalytic activity. *Biomass Convers. Biorefinery*, 2024.
- [6] Chitoria A.K., Mir A., Shah M.A. A review of ZrO_2 nanoparticles applications and recent advancements. *Ceram. Int.*, 2023, **49**, P. 32343–32358.

- [7] Arifin N.A., et al. Characteristic and challenges of scandia stabilized zirconia as solid oxide fuel cell material – In depth review. *Solid State Ion.*, 2023, **399**, 116302.
- [8] Zamudio-García J., et al. Exploring alkali metal doping in solid oxide cells materials: A comprehensive review. *Chem. Eng. J.*, 2024, **493**, 152832.
- [9] Danilenko I., et al. Do smaller oxide particles sinter worse? Paradoxes of the initial stages of sintering of zirconia nanoparticles. *Results Phys.*, **42**, 2022, 106027.
- [10] Du Z., et al. Size effects and shape memory properties in ZrO₂ ceramic micro- and nano-pillars. *Scr. Mater.*, 2015, **101**, P. 40–43.
- [11] Wang Y., et al. Failure analysis of fine-lamellar structured YSZ based thermal barrier coatings with submicro/nano-grains. *Surf. Coat. Technol.*, 2017, **319**, P. 95–103.
- [12] Sodeoka S., et al. Thermal and mechanical properties of ZrO₂–CeO₂ plasma-sprayed coatings. *J. Therm. Spray Technol.*, 1997, **6**, P. 361–367.
- [13] Chatterjee M., Naskar M.K., Ganguli D. Sol-emulsion-gel synthesis of alumina-zirconia composite microspheres. *J. Sol-Gel Sci. Technol.*, 2003, **28**, P. 217–225.
- [14] Liang S., et al. Scalable preparation of hollow ZrO₂ microspheres through a liquid-liquid phase reunion assisted sol-gel method. *Ceram. Int.*, 2020, **46**, P. 14188–14194.
- [15] Falcony C., Aguilar-Frutos M.A., García-Hipólito M. Spray pyrolysis technique; high-k dielectric films and luminescent materials: A Review. *Micromachines*, 2018, **9**, 414.
- [16] Liu L., et al. Supercritical hydrothermal synthesis of nano-ZrO₂: Influence of technological parameters and mechanism. *J. Alloys Compd.*, 2022, **898**, 162878.
- [17] Mosavari M., Khajehaghverdi A., Mehdiavaz Aghdam R. Nano-ZrO₂: A review on synthesis methodologies. *Inorg. Chem. Commun.*, 2023, **157**, 111293.
- [18] Buinachev S., et al. A new approach for the synthesis of monodisperse zirconia powders with controlled particle size. *Int. J. Hydrog. Energy*, 2021, **46**, P. 16878–16887.
- [19] Pasechnik L.A., et al. High purity scandium extraction from red mud by novel simple technology. *Hydrometallurgy*, **202**, 2021, 105597.
- [20] Chanturia V.A., Samusev A.L., Minenko V.G., Kozhevnikov G.A. Rare metal and rare earth recovery from silica gel-eudialyte concentrate leaching product. *J. Min. Sci.*, **57**, 2021, P. 1006–1013.
- [21] Vobenkaul D., et al. Hydrometallurgical processing of eudialyte bearing concentrates to recover rare earth elements via low-temperature dry digestion to prevent the silica gel formation. *J. Sustain. Metall.*, 2017, **3**, P. 79–89.
- [22] Pygay I.N., et al. Carbonization processing of bauxite residue as an alternative rare metal recovery process. *Tsvetnye Met.*, 2020, P. 56–63.
- [23] Xue Q., et al. Effects of Sc doping on phase stability of Zr_{1-x}Sc_xO₂ and phase transition mechanism: First-principles calculations and Rietveld refinement. *Mater. Des.*, 2017, **114**, P. 297–302.
- [24] Nakajima H., et al. Effects of Fe doping on crystalline and optical properties of yttria-stabilized zirconia. *J. Phys. Chem. Solids*, 2007, **68**, P. 1946–1950.
- [25] Hassan A.A.E., et al. Influence of alumina dopant on the properties of yttria-stabilized zirconia for SOFC applications. *J. Mater. Sci.*, 2002, **37**, P. 3467–3475.
- [26] Rong T.J., et al. State of magnesia in magnesia (10.4 mol %)-doped zirconia powder prepared from coprecipitation. *J. Am. Ceram. Soc.*, 2002, **85**, P. 1324–1326.
- [27] Danilenko I., et al. Determination of the nature of the co-doping effect on the structure, mechanical properties and ionic conductivity of SOFC electrolyte based on YSZ. *Solid State Ion.*, 2024, **412**, 116581.
- [28] Flegler A.J., et al. Cubic yttria stabilized zirconia sintering additive impacts: A comparative study. *Ceram. Int.*, 2014, **40**, P. 16323–16335.
- [29] Hbaieb K., et al. Reducing sintering temperature of yttria stabilized zirconia through addition of lithium nitrate and alumina. *Ceram. Int.*, 2012, **38**, P. 4159–4164.
- [30] Zhang X., et al. Structural evolution of Al-modified PS-PVD 7YSZ TBCs in thermal cycling. *Ceram. Int.*, 2019, **45** (6), P. 7560–7567.
- [31] Zhu D., et al. Furnace cyclic oxidation behavior of multicomponent low conductivity thermal barrier coatings. *J. Therm. Spray Technol.*, 2004, **13**, P. 84–92.
- [32] Fan W., et al. Improved properties of scandia and yttria co-doped zirconia as a potential thermal barrier material for high temperature applications. *J. Eur. Ceram. Soc.*, 2018, **38**, P. 4502–4511.
- [33] Zu J.H., et al. Preparation and high-temperature performance of Sc₂O₃–Y₂O₃ co-stabilized ZrO₂ thermal barrier coatings. *Ceram. Int.*, 2024, **50**, P. 20460–20472.

Submitted 13 September 2024; accepted 17 October 2024

Information about the authors:

Liliya A. Pasechnik – Institute of Solid State Chemistry UB RAS, Pervomayskaya, 91 Ekaterinburg 620108, Russia; ORCID 0000-0002-0631-5287; pasechnik@ihim.uran.ru

Irina S. Medyankina – Institute of Solid State Chemistry UB RAS, Pervomayskaya, 91 Ekaterinburg 620108, Russia; ORCID 0000-0002-8636-3755; lysira90@mail.ru

Danil I. Pereverzev – Institute of Solid State Chemistry UB RAS, Pervomayskaya, 91 Ekaterinburg 620108, Russia; ORCID 0000-0002-5678-4970; danil_per@mail.ru

Alexander Yu. Chufarov – Institute of Solid State Chemistry UB RAS, Pervomayskaya, 91 Ekaterinburg 620108, Russia; ORCID 0000-0003-3667-144X; cirulchufa@gmail.com

Alexey Yu. Suntsov – Institute of Solid State Chemistry UB RAS, Pervomayskaya, 91 Ekaterinburg 620108, Russia; ORCID 0000-0002-3488-1454; suntsov@ihim.uran.ru

Conflict of interest: the authors declare no conflict of interest.